energies

Article

Analysis of the Influence of the Skin Effect on the Efficiency and Power of the Receiver in the Periodic WPT System

Jacek Maciej Stankiewicz

Faculty of Electrical Engineering, Bialystok University of Technology, Wiejska 45D, 15-351 Bialystok, Poland; j.stankiewicz@doktoranci.pb.edu.pl

Abstract: The article shows an analysis of the influence of the skin effect on the maximum efficiency and maximum power of a receiver in a wireless power transfer system (WPT). For this purpose, the original solution of the WPT system was used, which contained periodically arranged planar coils. The results concern the multi-variant analysis of the WPT system. The geometry of the coils was taken into account, i.e., the size of coils, the number of turns, as well as the distance between the transmitting and receiving coils. The calculations were carried out over the frequency range of 0.1–1 MHz. In order to analyse the influence of the skin effect on the proposed WPT system, two approaches were used: analytical and numerical. The article analyses the appropriate selection of load impedance in order to obtain maximum efficiency or maximum power of the receiver. In this analysis, the influence of the skin effect on each of the two operating procedures was examined. The obtained analytical and numerical results differed by no more than 0.45%, which confirmed the correctness of the proposed WPT model. Based on the results, it was determined that the greatest influence of the skin effect occurred at 1 MHz. Then, the efficiency decreased by no more than 9%, while in the case of the receiver power decreased by an average of 25%. Detailed analysis shows the influence of the skin effect on the system parameters, and can also be an important element in the design of WPT systems.

Keywords: wireless power transfer; skin effect; numerical analysis; power and efficiency maximization; circuit analysis

Citation: Stankiewicz, J.M. Analysis of the Influence of the Skin Effect on the Efficiency and Power of the Receiver in the Periodic WPT System. *Energies* **2023**, *16*, 2009. https://doi.org/10.3390/en16042009

Academic Editor: ByoungHee Lee

Received: 27 December 2022
Revised: 13 February 2023
Accepted: 15 February 2023
Published: 17 February 2023

1. Introduction

Wireless power transfer (WPT) systems are used in many fields such as electric vehicle charging [1–4], electric vehicles (PHEVs) [5,6], implantable medical devices (IMDs) [7–9], and consumer electronics [10,11]. WPT technology is used in robotic systems [12], communication sets [13–15], and in the Internet of Things (IoT) [12,13]. WPT technology is divided into two main classes (Figure 1). The first is the radiated far-field WPT [16–18]. The second group is a non-radiated near-field WPT.

Many authors analysed the shape of the coils and winding methods. In [19], textile coils for near-field WPT were analysed due to their characteristics. The focus was on the efficiency of the WPT system. In [20], the authors analysed coils of various shapes (circular, square, or planar). In [21], the authors analysed sewn, laser cut, and printed inductors. One of the coils was made of silver-coated yarn. They showed that this type of coil was not suitable for the WPT system. The reason was the excessive resistance of the coil.

In WPT systems, there is an interaction between the magnetic field and the electric field. The AC current in the copper coils is the source of the magnetic field, which induces an oppositely directed electric field. This field is responsible for the formation of secondary currents, i.e., currents flowing in the conductor in the opposite direction to the main current. Secondary currents reduce the value of the magnetic field and change the current density. In addition, the magnetic field created by the current around the conductor affects the adjacent conductors, penetrating them as an electromagnetic wave, inducing currents on the surface of adjacent conductors and thus increasing the value of the current flowing. These phenomena are the source of the so-called skin effect. These phenomena have a significant influence on the value of power losses [22] and the efficiency of the entire WPT system. As the skin effect increases, so does the winding resistance [23]. To reduce power loss in copper, enameled wires are made into a bundle of wires made of many very thin conductors insulated from each other. The diameter of a single wire from which the bundle is made depends primarily on the depth of current penetration on the surface of the copper wire [23]. The wire diameter should be less than the penetration depth. This depth in a single copper wire depends on the frequency of change in current (f), permeability (μ), and conductivity (σ) of the conductor. At high frequencies, the skin effect causes the current not to flow through the entire cross-section of the wire, but only through its outer layer, adjacent to the surface, and the thickness of this layer decreases with increasing frequency.

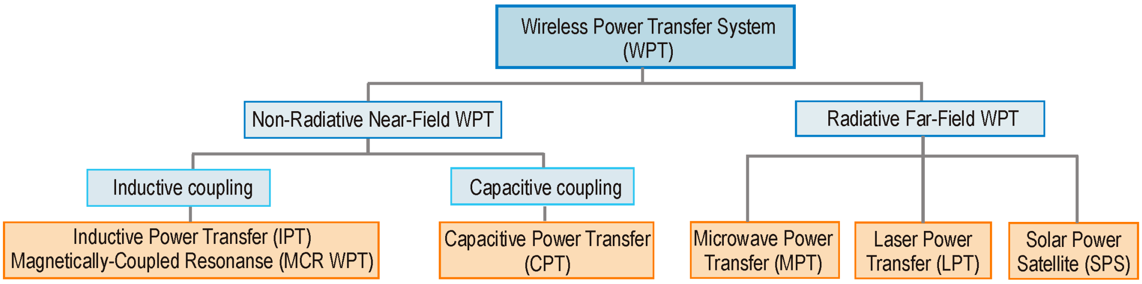

Figure 1. Classifications of the WPT system.

In [24], an optimized winding model was proposed. In this approach, a multi-strand Litz wire was used. This type of wire allows reducing the skin effect, particularly at high frequencies. Litz wire is one of the best solutions to reduce the skin effect. Unfortunately, it cannot be used for winding small planar coils, which are proposed in this article. For this reason, in small coils, it is important to know the influence of the skin effect on the efficiency of the system.

In [25], the skin effect at high frequency was studied. The authors showed a plane spiral arrangement with air hole. In this approach, they indicated that in order to reduce the influence of the skin effect, the thickness of the wire must be less than the skin depth. In [26], experimental measurements of the low frequency skin effect and internal inductance for a number of copper wires of various diameters and various linear cylindrical solid conductors, including copper, aluminum and brass rods, are provided. Measurements were compared with standard resistors, inductors, and capacitors.

Due to the problems related to the skin effect, new solutions are sought, including use of metamaterials [27] in WPT systems. In [28], the authors proposed the use of metasurfaces to enhance evanescent wave coupling to improve the wireless power transfer efficiency of multiple receivers.

Typical topologies are series and parallel combinations. In [29], the authors presented a series–parallel-series topology. This topology allows the power rating to be shifted in the event of severe misalignment. The authors [30] proposed various types of coils, e.g., domino. However, studies have only been conducted for the series configuration, when the series–parallel system has not yet been fully analysed.

Parallel connections have already been considered in the literature. For example, many sources and loads were shown in [31]. Nevertheless, to match the input impedance, the sources had been separated (in theory, each load had its own source), and additionally, the source—load connection was realized using intermediate resonant coils. This type of "modular" system has successfully integrated multiple low-power IPT systems to increase power level, even at the cost of efficiency. In [32], a different approach was used, several transmitter–receiver systems were made, but a single load was powered (similarly to [31]). Therefore, with a reduced number of parallel circuits and only one load, the matching network was not needed, while recent studies [33,34] focused on parallel-connected inverters (sources) with a single transmitting coil and one receiving coil. This resulted in the efficiency between 85% and 93%, whereas the study presented in this manuscript focused on both multiple sources and loads (arranged periodically) with the intention of powering low-power devices, which was not investigated widely so far.

The paper shows a WPT system with periodically arranged planar coils. Two analysis approaches (analytical and numerical) have been proposed. The analytical method allows quickly determining the main parameters of the system, such as power and efficiency. The proposed numerical solution does not require the entire model with all coils, as those presented in [35–37]. In typical numerical modeling of the WPT system, the authors did not use periodic boundary conditions. For this reason, the number of degrees of freedom (NDOF) is huge, which does not allow for detailed representation of the models and limits its size. The proposed numerical solution allows for the analysis of complex structures. Both proposed solutions reduce the size of numerical and circuit models. By appropriate selection of the load impedance, it was possible to calculate maximum efficiency and maximum load power. Therefore, the system was studied in two operating procedures. The analysis was conducted over the frequency range of 0.1 to 1 MHz. Calculations were made for different values of the model geometry. The influence of the skin effect and geometrical parameters of the WPT system on the efficiency and power of the load was analysed.

In Section 2, the analyzed model of the WPT system is presented and described. The author also describes numerical and analytical approaches to analysis. In Section 3, the following data are shown: (a) analysis conditions and calculated values of lumped parameters of the analyzed models (Section 3.1); (b) numerical and analytical results for the system operating at maximum efficiency (Section 3.2); (c) numerical and analytical results for the system operating at maximum load power (Section 3.3). In Section 4, the conclusions are described.

2. Analyzed Models Composed of Plane Coils

The considered system has transmitting (Tx) and receiving (Rx) coils. They are arranged periodically. Each Tx-Rx pair is called a WPT cell. The dimensions of the cell depend on the dimensions of the coils ($d \times d$) (Figure 2). Both coils (Tx and Rx) of the WPT have the same radius (r) and the same number of turns (n). Each coil contains an additional compensating capacitor. The transmitting coils form the transmitting surface and the receiving coils form the receiving surface, between which wireless energy transfer takes place. The transmitting surface has a sinusoidal voltage source (U_t). The receiving coils are connected to the loads (Z_l). Two types of coils were considered: a small coil (radius r = 0.01 m) and a large coil (radius r = 0.025 m). The coils were wound on a non-conductive carcass. Compensating capacitors are mounted on them, which are connected in series with the coils.

In the analyzed models, it is possible to select the power supply conditions depending on the requirements. Multiple receivers can be powered simultaneously. The considered cell $A_{x+\mathrm{m},y+\mathrm{n}}$ (Figure 2b) is part of an array, where m is the column number and n is the row number.

Each Tx is connected in parallel with a sinusoidal RMS voltage source (U_t), which powers the transmitting surface. Each WPT cell is assigned an individual load, which is $\underline{Z}_l$.

The article presents two approaches to analysis: numerical and analytical. The use of the proposed numerical approach allows reducing the number of degrees of freedom (NDOF) and shorten the analysis time (Section 2.1). However, the use of an analytical approach allows determining the power flow already at the design stage. A preliminary analysis of basic electrical properties is also possible (Section 2.2).

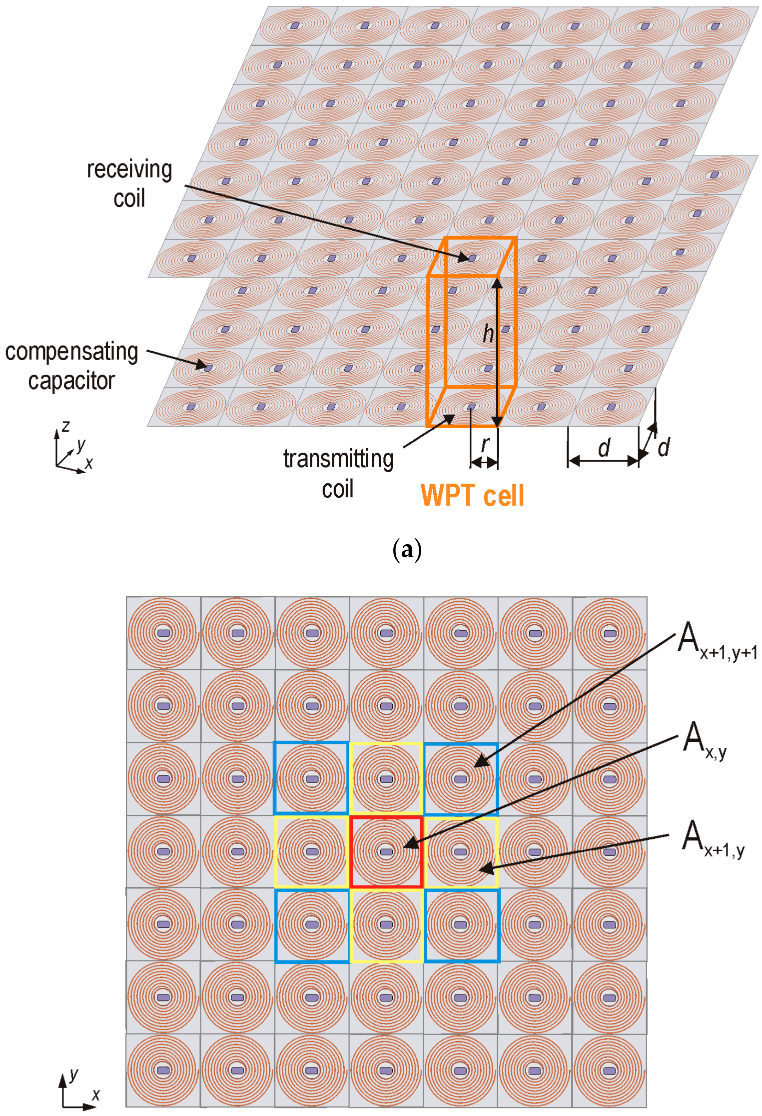

(**a**)

(**b**)

Figure 2. The analyzed periodic WPT system: (**a**) a three-dimensional model, (**b**) a two-dimensional fragment of a group of transmitting or receiving surfaces.

2.1. Numerical Approach

Numerical modeling is one of the basic tools of a scientist or engineer. With the use of appropriate models resulting from the approximate description of physical phenomena, it is possible to both test the design of devices and determine or optimize their essential features. The biggest challenge is to describe the problem, so that it is concise and contains the most important features of the modeled system. Proper selection of boundary conditions requires both practical experience and theoretical knowledge.

The use of numerical methods (e.g., FEM, FDTD, FDFD) [38–40] allows creating a model, and because of quick modifications, it is possible to perform a multi-variant analysis in order to determine the distribution of the magnetic field. The disadvantage of numerical methods is the limitation of the model geometry, i.e., the number of degrees of freedom (NDOF). In addition, the greater the number of degrees of freedom, the longer the computation time, but then the results are more accurate.

One of the most commonly used methods for building approximate numerical models is the finite element method (FEM). It allows searching for solutions of partial differential equations after discretization of these equations using mesh elements that are treated as fragments of a discretized area with homogeneous properties.

The COMSOL package, with the use of an additional *Radio Frequency* module, enables modeling of wave problems in the frequency domain. A detailed description of these boundary conditions can be found in the COMSOL package documentation [41,42].

The analyzed models had the following variables: coil radius (r), distance between the transmitting and receiving coils (h), and the number of turns (n). The coils are made of a very thin copper wire (w_d = 200 µm), an electrical insulator with a thickness (w_i = 5 µm), and wire conductivity (σ_c = 5.6 × 10^7 S/m). The analyzed cell is filled with air (Figure 3). The compensation capacitor was modelled as a lumped element with capacitance (C). With periodic boundary conditions (PBC) [38–42], it is possible to simplify the model to a single cell filled with air and composed of a Tx-Rx pair. Periodic conditions were provided on surfaces parallel to the Z-axis. Using the finite element method, the entire area needs to be digitized. A perfectly matched layer (PML) was used to simulate an unrestricted environment, which prevents wave reflections from the boundaries of the area. Two additional layers (PML) were introduced at the top and bottom of the WPT cell (Figure 3a).

In addition, taking into account the use of the finite element method, the discretization of the area must be matched to the electromagnetic wave generated in it. In order to correctly represent the wave character in the considered models, the size of the mesh elements was selected, so that there were at least 20 elements between adjacent nodes per wavelength [40–42] (Figure 3b,c). A smaller number does not allow good mapping of the entire wave period, while a larger number increases the number of degrees of freedom, which also extends the calculation time.

The proposed model of the WPT system was constructed in the *Comsol Multiphysics 4.3b* software, which has built-in functions to solve the presented problems. It was possible to limit the number of degrees of freedom by using the finite element mesh adaptation. This allowed the mesh to be fine-tuned at important points in the model, i.e., coil turns and corners, for accurate results. The mesh inside the model consisted of elements such as *Free tetrahedral* and *Free triangular*. An analysis was conducted in the frequency domain, taking into account the physics of *Magnetic fields* in connection with a fragmentary *Equivalent circuit*. The coils were modeled using the built-in current sheet approximation of planar inductors (*Multi-turn coil boundary condition*), where the voltage source (U_t = 1 V), capacitors (C), and load (Z_l) were connected to the coils by internal coupling with a fragmentary *Equivalent circuit*. The numerical models contained approximately 500,000 degrees of freedom.

The energy transport problem can be calculated using a magnetic vector potential

$$\mathbf{A} = [\mathbf{A}_x \; \mathbf{A}_y \; \mathbf{A}_z], \tag{1}$$

and the Helmholtz equation

$$\nabla \times \left(\frac{1}{\mu_0} \nabla \times \mathbf{A} \right) - \mathrm{j}2\pi f \sigma \mathbf{A} = \mathbf{J}_e, \tag{2}$$

where $\mathbf{J}_e$ is an external current density [A/m^2] that results from a voltage supply (U_t). Equations (1) and (2) were solved by finite element method (FEM) [40–43]. The periodic boundary conditions on the four external surfaces were defined as magnetic insulation $\mathbf{n}_s \times \mathbf{A} = 0$, where $\mathbf{n}_s$ is a surface normal vector $\mathbf{n}_s = [\mathbf{1}_x \; \mathbf{1}_y \; \mathbf{1}_z]$.

The analyzed models of WPT system are presented in Table 1. The calculations were performed over a specified frequency range of 0.1 MHz to 1 MHz with a step of 50 kHz, at the distances $h = r/2$ and $h = r$ for the small and large coils.

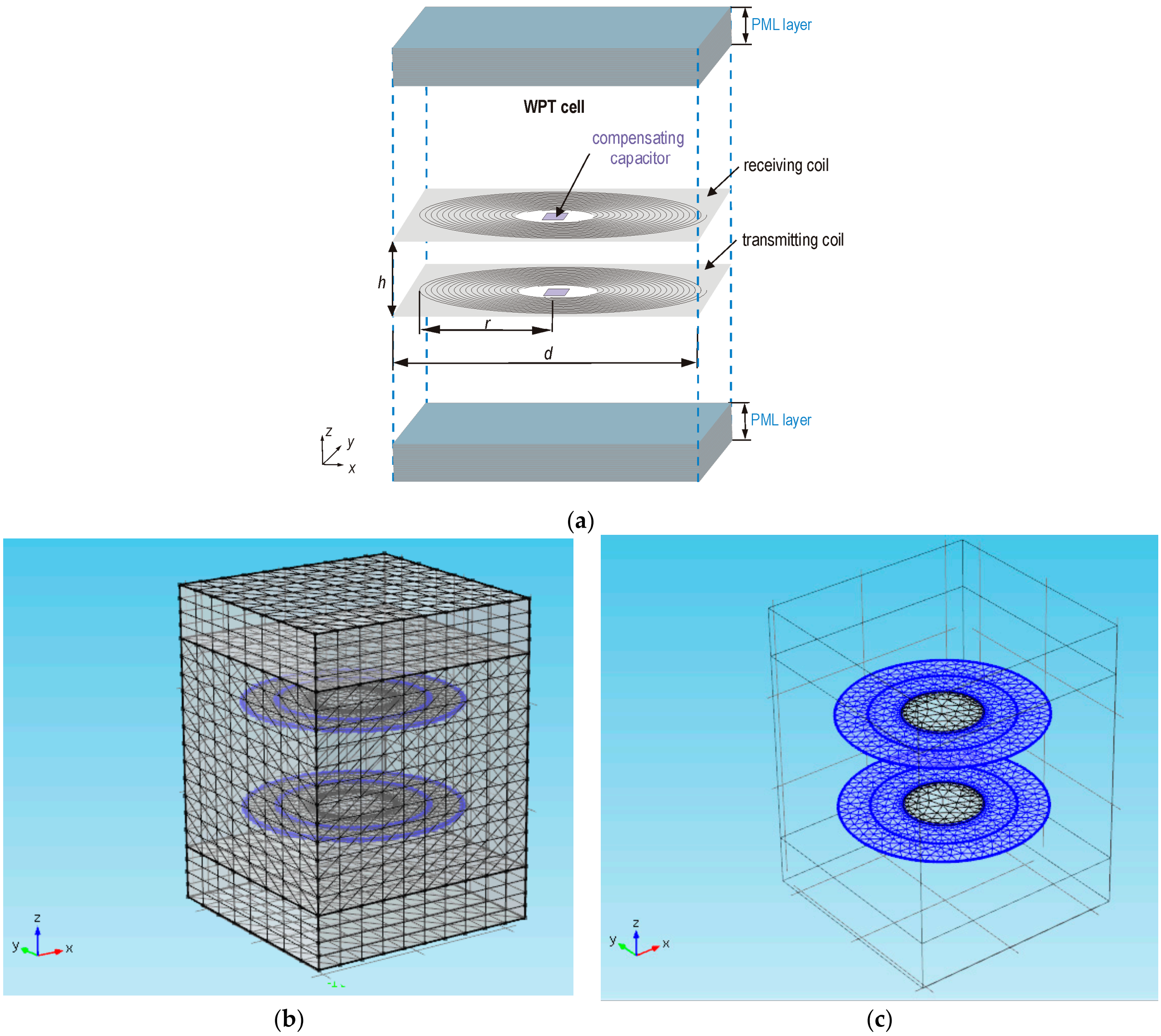

Figure 3. A numerical model with a pair of coils Tx-Rx: (**a**) a WPT cell geometry, (**b**) a grid over the entire area, (**c**) a grid over coils.

Table 1. Geometrical parameters of the analyzed models of WPT system.

r **(m)**	***n***	***h*** **(m)**	
0.01	10	0.005	0.01
	20	0.005	0.01
	30	0.005	0.01
	40	0.005	0.01
0.025	50	0.0125	0.025
	60	0.0125	0.025
	70	0.0125	0.025

2.2. Analytical Approach

Numerical methods provide correct results if appropriate boundary conditions are applied and the real model is well mapped. Unfortunately, in numerical modeling it is often necessary to use simplifications, e.g., to reduce NDOF. On the other hand, the implementation of the equivalent circuit and the use of analytical equations allow obtaining a solution related to power transport. Very often, a simpler model that still provides the same range of calculations is desired. The use of the analytical method allows avoiding the long modeling process with the imposed requirements of the numerical method [43].

Due to the developed analytical method, it is possible to reduce a wide periodic network to a single WPT cell (Figure 4a). This approach will allow determining the initial results of the analysis, but at the same time, it is less complicated and does not require numerical modeling. The proposed analytical solution is a combination of a two-port set with a dependency for determining lumped parameters. The solution in the frequency domain was performed using circuit analysis (Figure 4b). In this case, the problem is to determine the lumped parameters taking into account the influence of the adjacent coils on the equivalent inductances Tx and Rx and mutual inductance M_t.

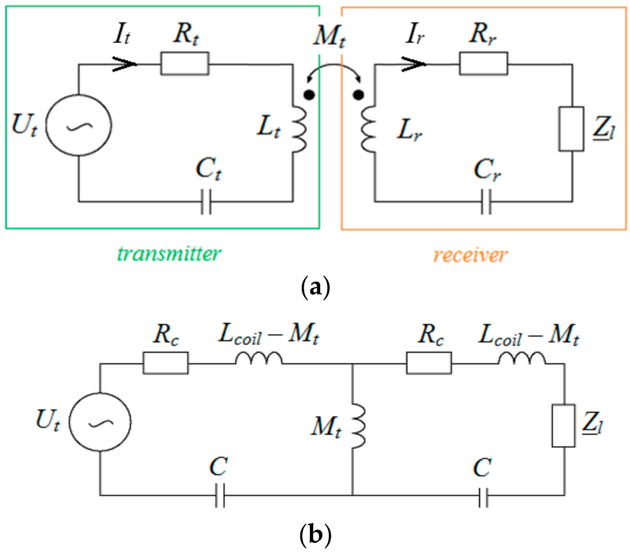

Figure 4. An analytical model with (**a**) a periodic cell, (**b**) a replacement circuit.

In an analytical approach, there are mutual inductances between adjacent coils, which influence the inductance in $A_{x,y}$ that is presented by

$$L_{coil} = L_s + \sum_m \sum_n M_{x+m,y+n}. \tag{3}$$

L_{coil} is an effective self-inductance [H], $M_{x+m,y+n}$—mutual inductance between coils [H], L_s—self-inductance of a spiral coil [H], which is described by

$$L_s = \frac{\mu_0 k_1 d_m n^2}{2}\left[\ln\left(\frac{k_2}{\alpha}\right) + k_3\alpha + k_4\alpha^2\right]. \tag{4}$$

A mean diameter is presented by

$$d_m = \frac{2r + 2[r - n(w_d + d_i)]}{2}. \tag{5}$$

A fill factor is described by

$$\alpha = \frac{n(w_d + w_i)}{2r - n(w_d + w_i)}. \tag{6}$$

Coefficients k_1, k_2, k_3, k_4 depend on the shape of the coil [44]. Then, Equation (3) can be presented as

$$L_{coil} = L_s + M_p, \tag{7}$$

where M_p is the sum of mutual inductances in the periodic grid, because it reduces the inductance of the coil, it is with a minus. When the load $Z = \infty$ and there is no capacitor in series with Tx, M_p is calculated as

$$M_p = \frac{\frac{U_t}{I_{t,\infty}} - R_c}{\mathrm{j}\omega} - L_s, \tag{8}$$

where R_c—coil resistance [Ω], $\underline{I}_{t,\infty} = |\underline{I}_{t,\infty}| e^{\mathrm{j}\psi}$—source current [A]. To avoid calculating each $M_{t,x+m,y+n}$, M_t is solved by dependence

$$M_t = \frac{\frac{U_{r,\infty}}{I_{t,\infty}}}{\mathrm{j}\omega}, \tag{9}$$

where $\underline{U}_{r,\infty} = |\underline{U}_{r,\infty}| e^{\mathrm{j}\theta}$—voltage induced in the receiving coil [V]. After self-inductance (L_s) and mutual inductance (M_p) were calculated, the series resonant capacitance was determined (C):

$$C(f) = \frac{1}{\omega^2 L_{coil}} = \frac{1}{\omega^2 (L_s + M_p)}. \tag{10}$$

For the wire width ($w_d + w_i$), the total length is obtained by

$$l_{sm} = 2\pi n \left[r - \frac{(n-1)(w_d + w_i)}{2} \right]. \tag{11}$$

Taking into account that the transmitter and receiver coils are identical, the resistances of the inductors are $R_t = R_r = R_c$. The formulas for R_c for the case without the skin effect, Equation (12), and for the case with the skin effect, Equation (13), are presented by

$$R_c = \frac{l_{sm}}{\sigma_c \pi \frac{w_d^2}{4}}, \tag{12}$$

$$R_{c\_ac} = \frac{l_{sm}}{\sigma_c a_w} = \frac{2\pi n \left[r - \frac{(n-1)(w_d + w_i)}{2} \right]}{\sigma_c a_w}, \tag{13}$$

where σ_c—conductivity of the wire [S/m], a_w—the effective cross-section of the wire [m^2], Equation (14):

$$a_w = \pi \left(w_d \delta_e - \delta_e^2 \right), \tag{14}$$

where δ_e is the effective skin depth [m] [45] which is described by

$$\delta_e = \delta \left(1 - \exp\left(\frac{-w_d}{2\delta} \right) \right). \tag{15}$$

At the same time, δ is the skin depth:

$$\delta = \sqrt{\frac{1}{\pi f \sigma_c \mu_0}}. \tag{16}$$

3. Analysis of the Calculated Values Obtained by Two Methods

3.1. Analysis Conditions and Calculated Values of Lumped Parameters

Both methods were used in the analysis with the same parameters (Section 2.1). The analyzed WPT system models are presented in Table 1.

The same values were used for analytical calculations as in the numerical simulation, e.g., w_d = 200 μm, w_i = 5 μm, $\sigma_c = 5.6 \times 10^7$ S/m, and U_t = 1 V. On the basis of the values presented above, the correctness of the adopted assumptions was assessed. For this purpose, a comparison of the active power of the receiver (P_r) and the power of the transmitter (P_t) was conducted:

$$P_r = R_o I_r^2, \tag{17}$$

$$P_t = U_t I_t. \tag{18}$$

The power transfer efficiency was calculated as

$$\eta = \frac{P_r}{P_t} 100\%. \tag{19}$$

The analysis was related with the suitable choice of the impedances by Equations (20)–(23) over an analyzed frequency range:
-for the procedure with maximum efficiency:

$$Z_{eff} = \sqrt{R_c{}^2 + (\omega M_t)^2}, \tag{20}$$

and in the case of the skin effect

$$Z_{eff\_ac} = \sqrt{R_{c\_ac}{}^2 + (\omega M_t)^2}. \tag{21}$$

-for the procedure with maximum load power:

$$Z_{pow} = R_c + \frac{\omega^2 M_t{}^2}{R_c}, \tag{22}$$

and in the case of the skin effect

$$Z_{pow\_ac} = R_{c\_ac} + \frac{\omega^2 M_t{}^2}{R_{c\_ac}}. \tag{23}$$

The lumped parameters of the electrical circuit were determined using Equations (12)–(13), (20)–(23). The values of the WPT system used in the analysis are presented in Tables 2–5. When n increases, both impedances and the coil resistance increase. The skin effect increases the coil resistance and impedance Z_{eff}. On the other hand, it causes a decrease in the impedance Z_{pow}.

Table 2. Calculated circuit parameters for r = 0.01 m (without skin effect).

n	R_c (Ω)	Z_{eff} (Ω) at 1 MHz		Z_{pow} (Ω) at 1 MHz$_x$	
		h = 0.005 m	h = 0.01 m	h = 0.005 m	h = 0.01 m
10	0.32	2.42	0.63	18.01	1.21
20	0.58	8.73	2.08	133	7.54
30	0.75	15.26	3.61	310	17.33
40	0.86	18.69	4.39	408	22.52

Table 3. Calculated circuit parameters for r = 0.025 m (without skin effect).

n	R_c (Ω)	Z_{eff} (Ω) at 1 MHz		Z_{pow} (Ω) at 1 MHz	
		h = 0.0125 m	h = 0.025 m	h = 0.0125 m	h = 0.025 m
50	3.57	137	31.54	5219	279
60	4.06	180	41.71	7951	428
70	4.48	218	50.75	10627	575

Table 4. Calculated circuit parameters for r = 0.01 m (with skin effect).

n	R_{c_ac} at 1 MHz (Ω)	Z_{eff_ac} (Ω) at 1 MHz		Z_{pow_ac} (Ω) at 1 MHz	
		h = 0.005 m	h = 0.01 m	h = 0.005 m	h = 0.01 m
10	0.42	2.43	0.68	14	1.10
20	0.75	8.74	2.14	102	6.11
30	0.98	15.28	3.67	239	13.74
40	1.11	18.71	4.45	314	17.79

Table 5. Calculated circuit parameters for r = 0.025 m (with skin effect).

n	R_{c_ac} at 1 MHz (Ω)	Z_{eff_ac} (Ω) at 1 MHz		Z_{pow_ac} (Ω) at 1 MHz	
		h = 0.0125 m	h = 0.025 m	h = 0.0125 m	h = 0.025 m
50	4.63	137	31.67	4021	217
60	5.27	180	41.85	6124	332
70	5.82	218	50.88	8188	445

3.2. System Operating with the Maximum Power Transfer Efficiency

In this section, the calculation results of the analyzed WPT system, obtained by analytical and numerical methods, were compared. The parameters of the system (r, n, and h) were taken into account. Transmitter, receiver powers, and efficiency were calculated based on both models.

In the maximum efficiency procedure, the impedances of the receiver Z_{eff} and Z_{eff_ac} were calculated based on Equations (20) and (21). Calculations for different n and h are shown in Figure 5 for a small coil and in Figure 6 for a large coil. The analysis showed that the influence of the skin effect on the impedance values was negligible. Increasing n causes a linear increase in impedance for a coil of r = 0.025 m and a non-linear increase for a coil of r = 0.01 m. Regardless of the coil size, doubling h causes an approximately four-time decrease in the impedance.

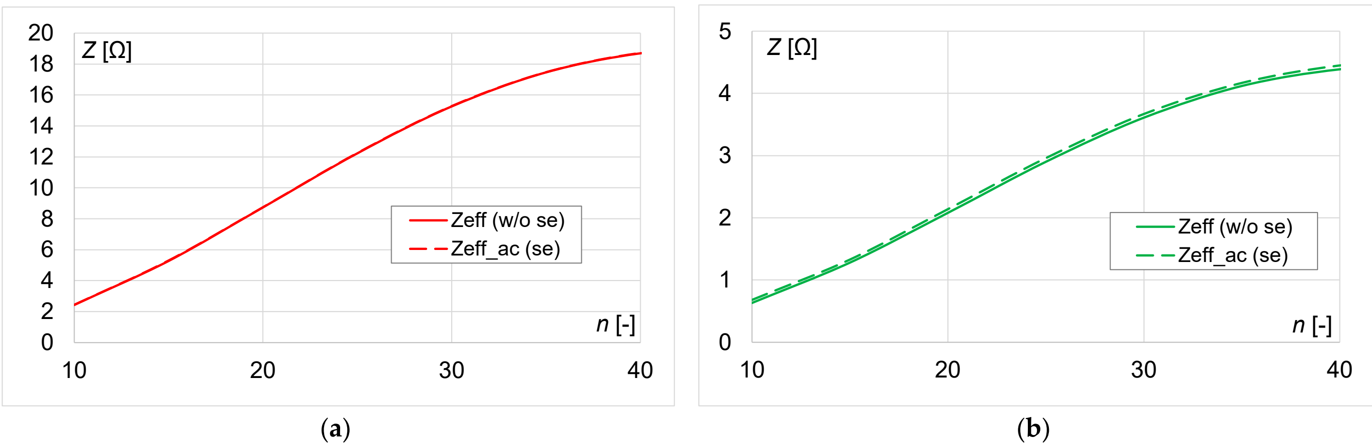

Figure 5. Load impedance for the cases with and without skin effect at 1 MHz for the small coil at (**a**) h = 0.005 m; (**b**) h = 0.01 m.

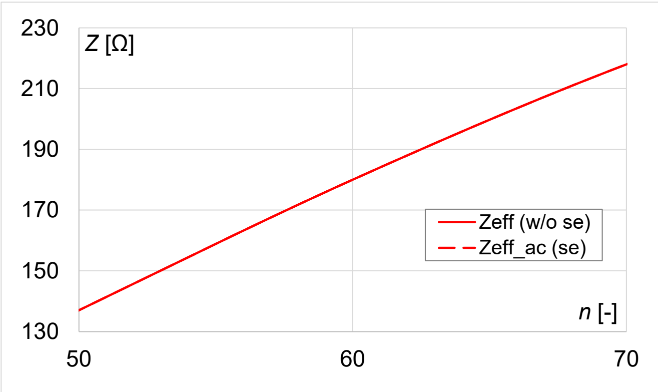

(**a**)

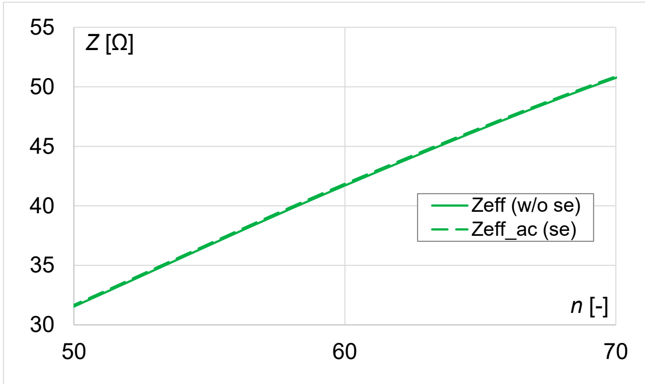

(**b**)

Figure 6. Load impedance for the cases with and without skin effect at 1 MHz for the large coil at (**a**) $h = 0.0125$ m; (**b**) $h = 0.025$ m.

In Figure 7, the resistances of coils are presented ($r = 0.01$ m and $r = 0.025$ m). Skin effect increases coil resistance by approx. 30% for small and large coils and regardless of the number of turns.

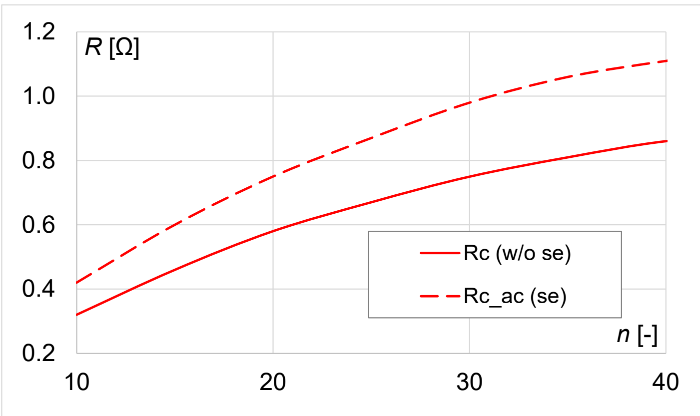

(**a**)

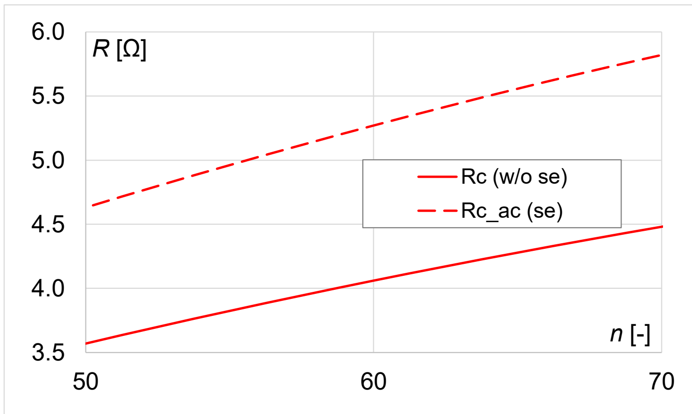

(**b**)

Figure 7. Coil resistance with skin effect at 1 MHz and without skin effect for (**a**) small coil; (**b**) large coil.

Maximum η values were compared, depending on n and h, for cases with and without skin effect, as seen in Table 6. Increasing the number of turns and/or the radius of the coil increases the efficiency of the system. An increase in h causes a decrease in system efficiency for the same coil size.

Higher η was obtained for the case without the skin effect. The results from numerical and analytical methods were compared. For each case, absolute error was calculated, which did not exceed 0.45%. It proved that the results were consistent.

The greatest influence of the skin effect on the efficiency occurs for a small coil, regardless of the distance h, at 9% (Table 7).

Table 6. Maximum power transfer efficiency values at 1 MHz.

n	η (%) at 1 MHz			
	With Skin Effect		Without Skin Effect	
	h = 0.005 m	h = 0.01 m	h = 0.005 m	h = 0.01 m
10	70.48	23.62	76.43	31.77
20	84.26	48.19	87.72	56.81
30	87.97	57.89	90.66	65.28
40	88.76	59.98	91.31	67.07
	h = 0.0125 m	h = 0.025 m	h = 0.0125 m	h = 0.025 m
50	93.43	74.11	94.90	79.35
60	94.31	77.66	95.59	82.28
70	94.83	79.18	95.99	83.48

Table 7. Difference between the maximum values of η at 1 MHz for cases with and without skin effect.

n	Δ_η (%) at 1 MHz	
	h = 0.005 m	h = 0.01 m
10	6	8
20	3	9
30	3	7
40	3	7
	h = 0.0125 m	h = 0.025 m
50	1	5
60	1	5
70	1	4

The P_t, P_r power, and η characteristics are shown on the graphs: in Section 3.2.1 for the small coil and in Section 3.2.2 for the large coil. The numerical analysis results are presented as dashed lines for the case with the skin effect and solid lines for the case without the skin effect (marked as FEM in the legend). The results of the analytical analysis are represented by dots (marked as A in the legend).

3.2.1. Results for a Small Coil

The graphs: transmitter, receiver power, and efficiency at the distances between the coils h = 0.005 m and h = 0.01 m for cases with and without skin effect are presented in Figures 8–11.

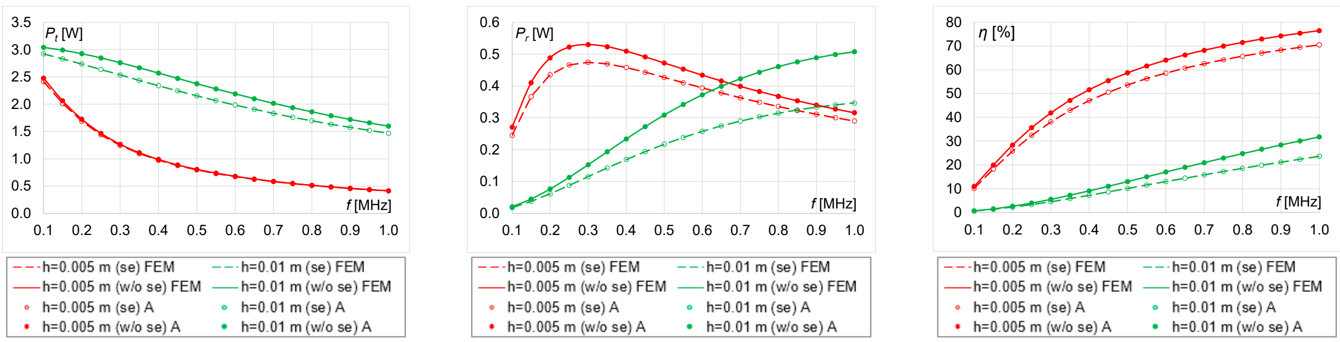

(**a**) (**b**) (**c**)

Figure 8. Results for n = 10 for the cases with and without skin effect: (**a**) P_t, (**b**) P_r, (**c**) η.

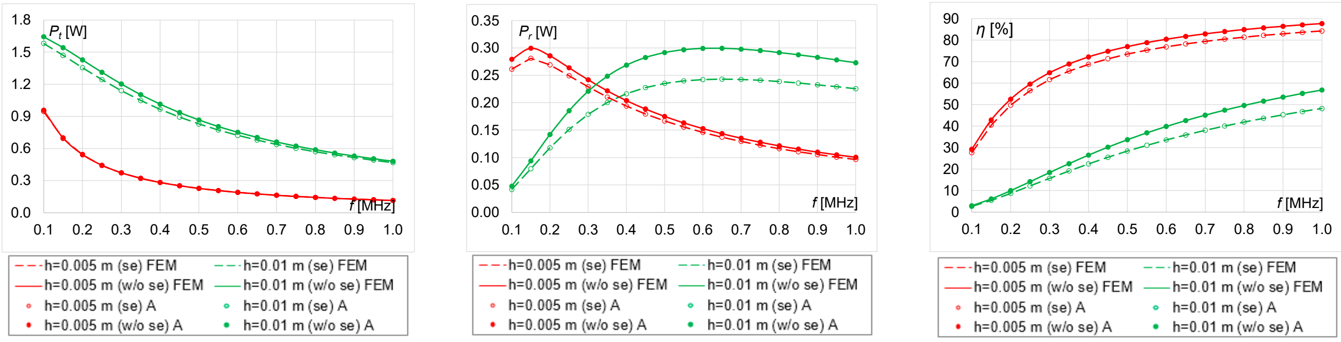

(**a**) (**b**) (**c**)

Figure 9. Results for n = 20 for the cases with and without skin effect: (**a**) P_t, (**b**) P_r, (**c**) η.

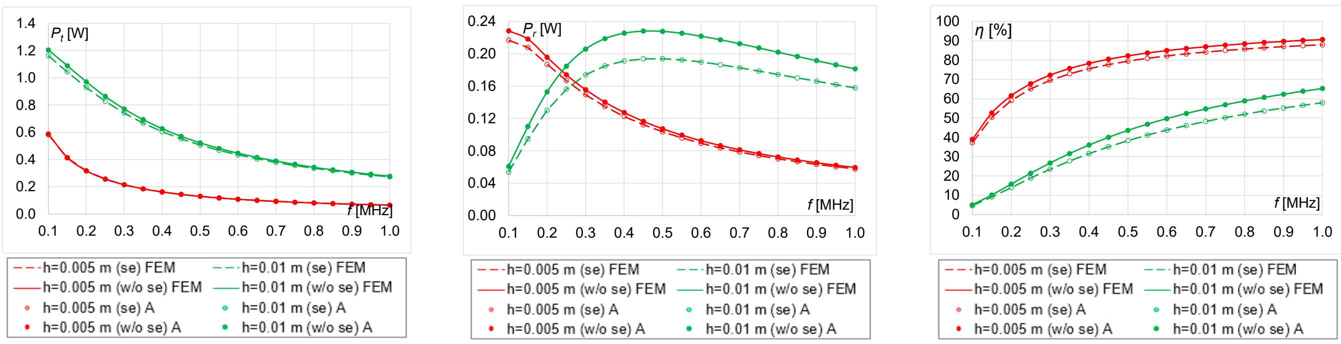

(**a**) (**b**) (**c**)

Figure 10. Results for n = 30 for the cases with and without skin effect: (**a**) P_t, (**b**) P_r, (**c**) η.

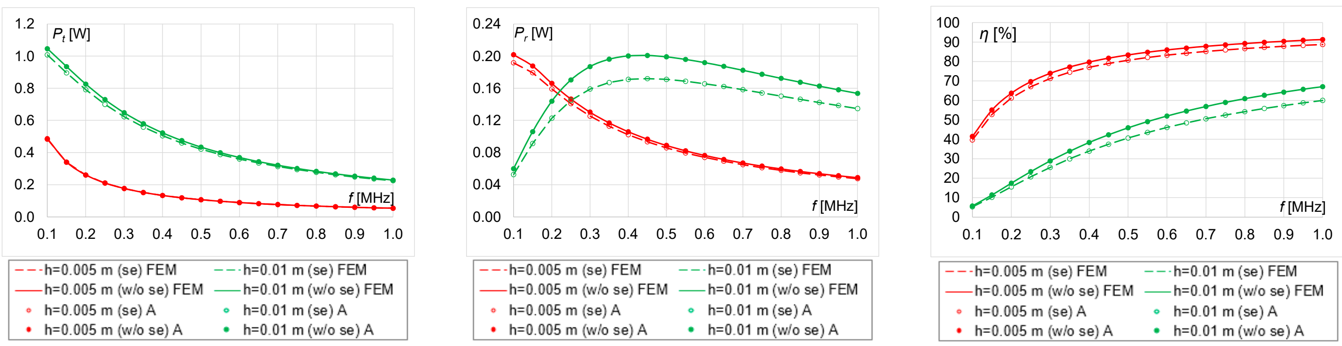

(**a**) (**b**) (**c**)

Figure 11. Results for n = 40 for the cases with and without skin effect: (**a**) P_t, (**b**) P_r, (**c**) η.

The P_t power decreases over the entire frequency range, regardless of n (Figures 8a, 9a, 10a and 11a). This power is the same for the cases with and without skin effect at h = 0.005 m. However, at h = 0.01 m, P_t is higher for the case without skin effect, regardless of n.

Receiver power is always higher for the case without skin effect (Figures 8b, 9b, 10b and 11b). The greatest differences in values occur at h = 0.01 m and equal 150 mW for n = 10 at 1 MHz (Figure 8b). When η reaches approx. 50%, the P_r power reaches its maximum value. Then, the power decreases. The P_r power decreases with increasing n.

As the frequency increases, η increases, too, regardless of h and n (Figures 8c, 9c, 10c and 11c). Doubling the distance h results in a decrease in efficiency by up to 40%. The greatest difference in efficiency η, for the cases with and without skin effect, occurs at h = 0.01 m, n = 20 and reaches 9% at the frequency of 1 MHz (Figure 9c). As n increases, this difference decreases.

3.2.2. Results for a Large Coil

Figures 12–14 present the graphs: P_t, P_r power, and efficiency at h = 0.0125 m and h = 0.025 m, for the cases with and without skin effect.

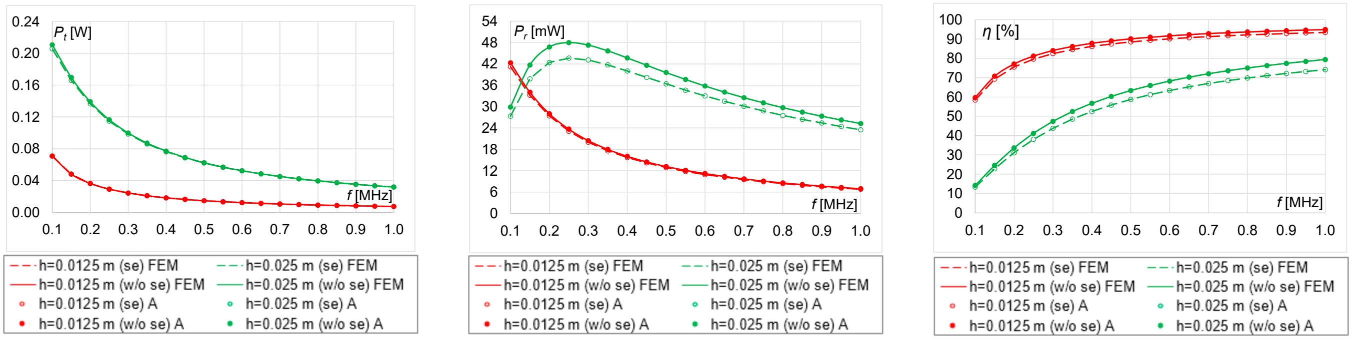

(**a**) (**b**) (**c**)

Figure 12. Results for n = 50 for the cases with and without skin effect: (**a**) P_t, (**b**) P_r, (**c**) η.

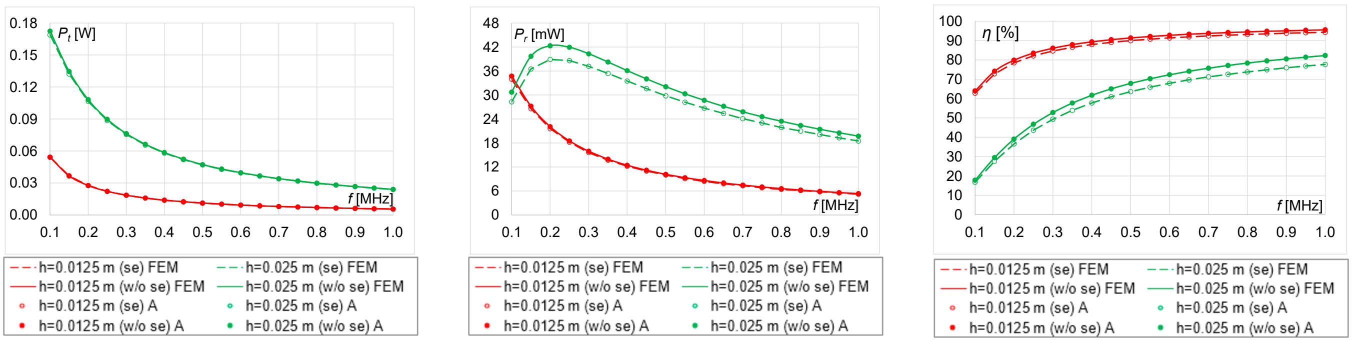

(**a**) (**b**) (**c**)

Figure 13. Results for n = 60 for the cases with and without skin effect: (**a**) P_t, (**b**) P_r, (**c**) η.

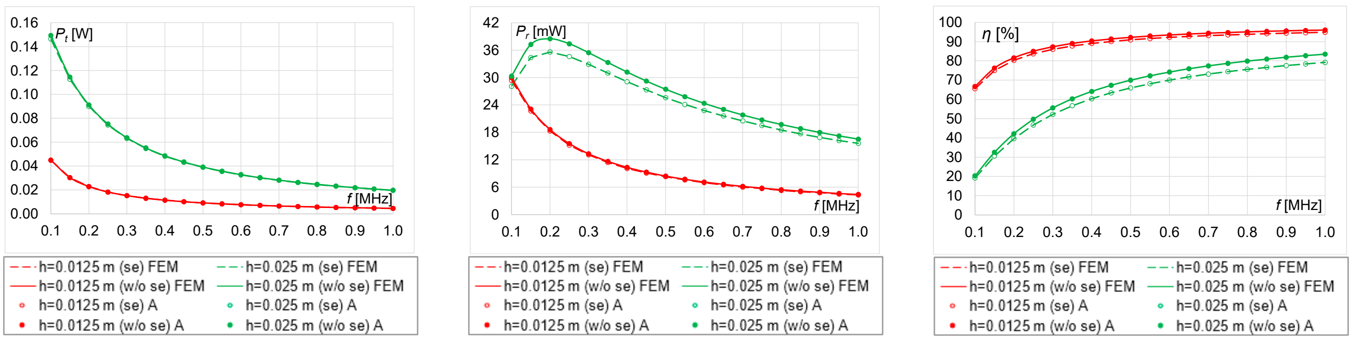

(**a**) (**b**) (**c**)

Figure 14. Results for n = 70 for the cases with and without skin effect: (**a**) P_t, (**b**) P_r, (**c**) η.

The P_t power decreases over the entire frequency range, regardless of n and h (Figures 12a, 13a and 14a). The transmitter power is always higher at h = 0.025 m, regardless of n. The greatest difference in values occurs in the lower frequency range. The P_t power is the same for the cases with and without skin effect at all distances.

At the distance h = 0.025 m, it can be observed that with all characteristics, when the efficiency reaches approx. 50%, the P_r power reaches its maximum value (Figures 12b, 13b and 14b). Then, this power decreases when the efficiency exceeds 50%. The P_r power is higher at h = 0.025 m over the entire frequency range. As n increases, the P_r power decreases. The shape of the P_r characteristics for the cases with and without skin effect is very similar. The receiver power is always higher for the case without skin effect. Regardless of the distance h, this difference decreases with the increase in n over the entire range of the analyzed frequencies.

As the frequency increases, η increases, too, regardless of h and n (Figures 12c, 13c and 14c). Doubling the distance h resulted in a decrease in η by up to 50% at lower frequencies. The greatest difference in η for the cases with and without skin effect occurs at h = 0.025 m and reaches 4–5%. At h = 0.0125 m, the difference is negligible, at 1%, regardless of n. The shape of the efficiency characteristics for all cases is very similar.

3.3. System Operating with the Maximum Load Power

In the maximum load power procedure, the values of the load impedances Z_{pow} and Z_{pow_ac} were calculated, taking into account n, the distance h between the coils Tx and Rx, for the small coil (Figure 15) and the large coil (Figure 16).

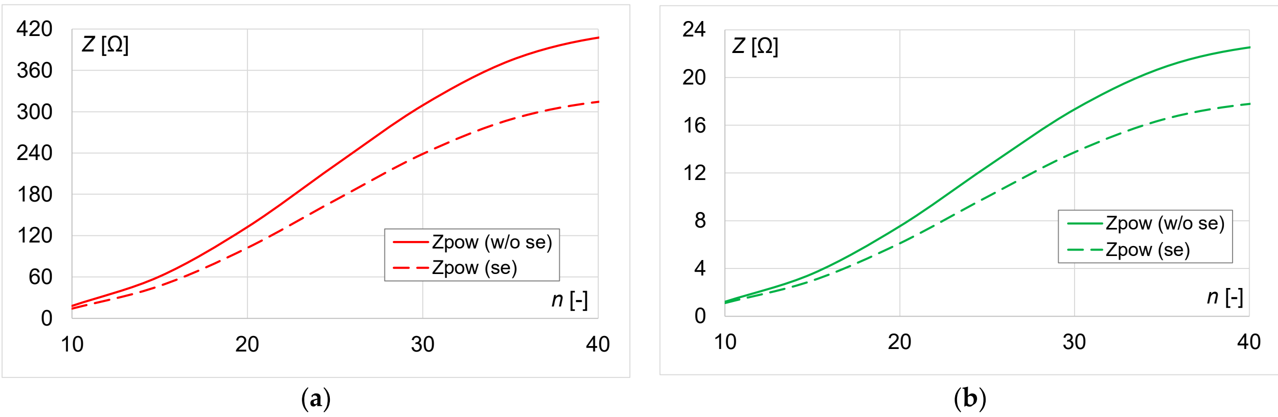

Figure 15. Load impedance for the cases with and without skin effect at 1 MHz for the small coil at (**a**) h = 0.005 m; (**b**) h = 0.01 m.

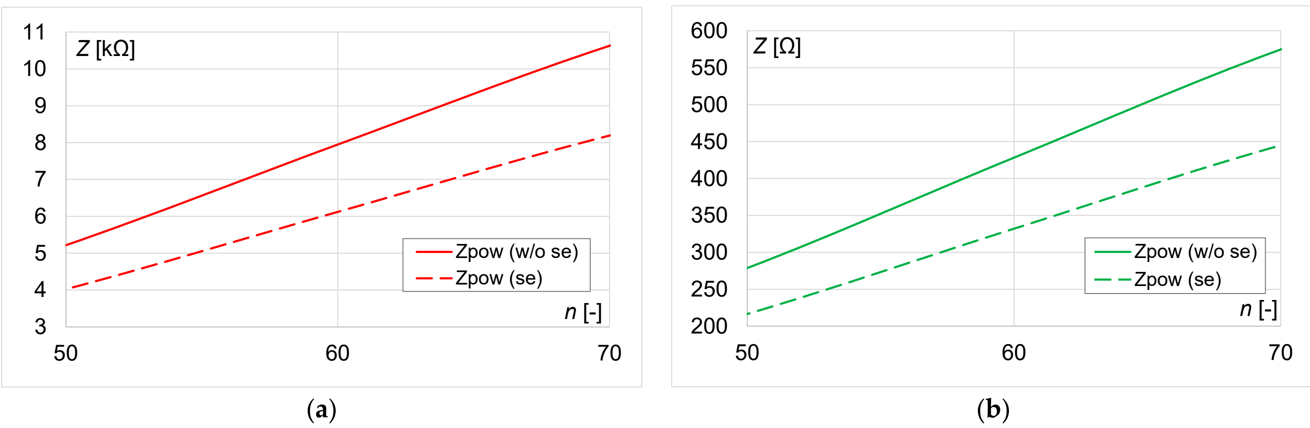

Figure 16. Load impedance for the cases with and without skin effect at 1 MHz for the large coil at (**a**) h = 0.0125 m; (**b**) h = 0.025 m.

Doubling h results in over than eighteen-time decrease in the impedance for the small coil and over than seventeen-time decrease for the large coil. The influence of the skin effect on the impedance values was the highest for n = 40 for the small coil and for n = 70 for the large coil; it was above 20% in both cases.

Maximum load power values, depending on n and h, were compared for cases with and without skin effect, as seen in Table 8.

Table 8. Maximum load power values at 1 MHz.

n	P_r (mW) at 1 MHz			
	With Skin Effect		**Without Skin Effect**	
	h = 0.005 m	h = 0.01 m	h = 0.005 m	h = 0.01 m
10	578	369	756	564
20	333	295	433	402
30	255	238	332	318
40	225	211	292	282
	h = 0.0125 m	h = 0.025 m	h = 0.0125 m	h = 0.025 m
50	54	53	70	69
60	47	47	62	61
70	43	43	56	56

Higher load power values were obtained for the case without skin effect. The greatest influence of the skin effect on P_r power was observed for the small coil at h = 0.01 m and n = 10, but for the large coil it was observed for n = 50 (Table 9).

Table 9. Difference between the maximum load power values at 1 MHz for cases with and without skin effect.

n	ΔP_r (mW) at 1 MHz	
	h = 0.005 m	h = 0.01 m
10	178	195
20	100	107
30	77	80
40	67	71
	h = 0.0125 m	h = 0.025 m
50	16	16
60	15	14
70	13	13

The results obtained by circuit and numerical methods were compared. For each case, the absolute error was calculated, which did not exceed 2.4 mW. It proved that the results were consistent.

The P_t, P_r power, and η characteristics are shown on the graphs: in Section 3.3.1 (r = 0.01 m) (Figures 17–20) for the small coil and in Section 3.3.2 (r = 0.025 m) (Figures 21–23) for the large coil. The numerical analysis results are presented as dashed lines for the case with the skin effect and solid lines for the case without the skin effect (marked as FEM in the legend). The results of the analytical analysis are represented by dots (marked as A in the legend).

3.3.1. Results for a Small Coil

The transmitter, receiver power, and efficiency graphs at the distances h = 0.005 m and h = 0.01 m for the cases with and without skin effect are presented in Figures 17–20.

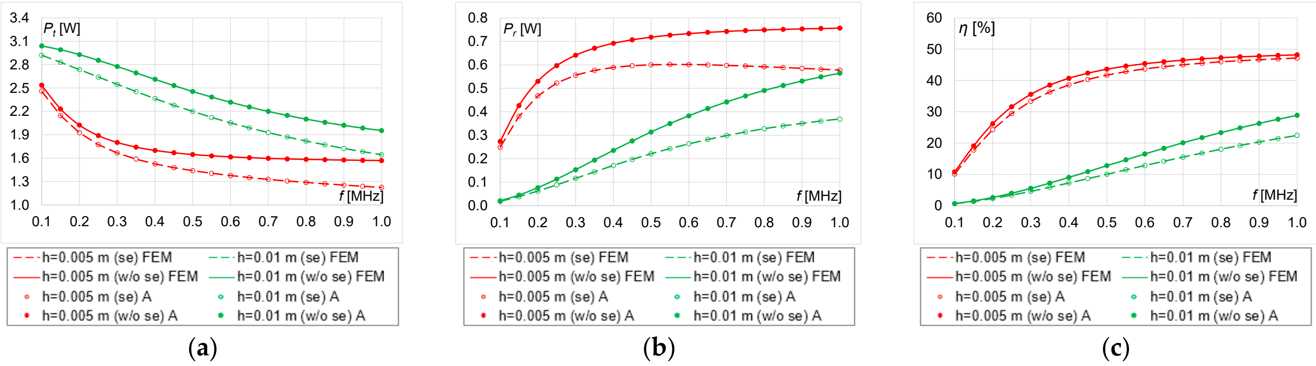

Figure 17. Results for n = 10 for the cases with and without skin effect: (**a**) P_t, (**b**) P_r, (**c**) η.

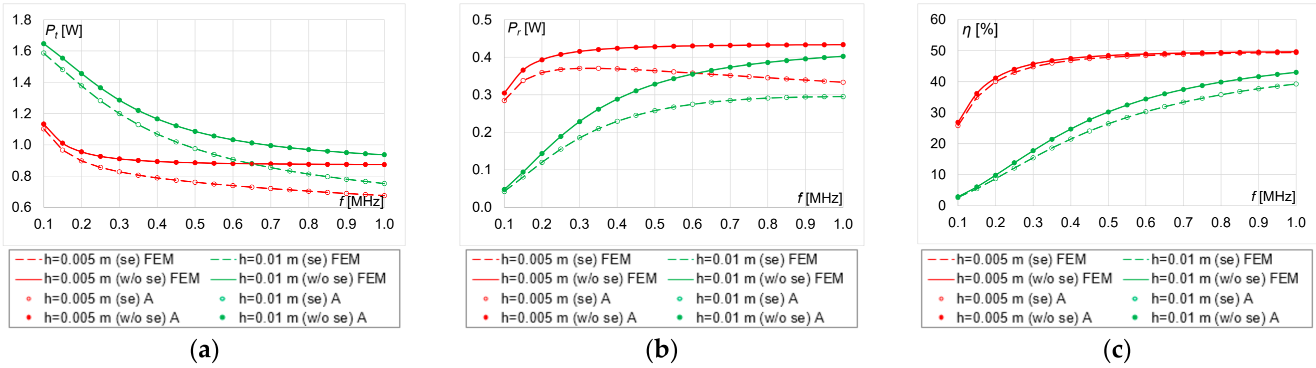

Figure 18. Results for n = 20 for the cases with and without skin effect: (**a**) P_t, (**b**) P_r, (**c**) η.

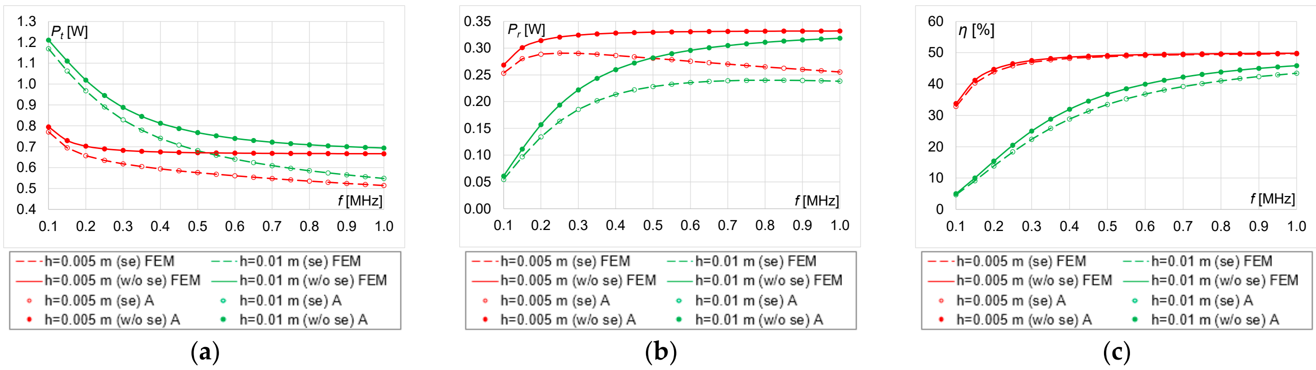

Figure 19. Results for n = 30 for the cases with and without skin effect: (**a**) P_t, (**b**) P_r, (**c**) η.

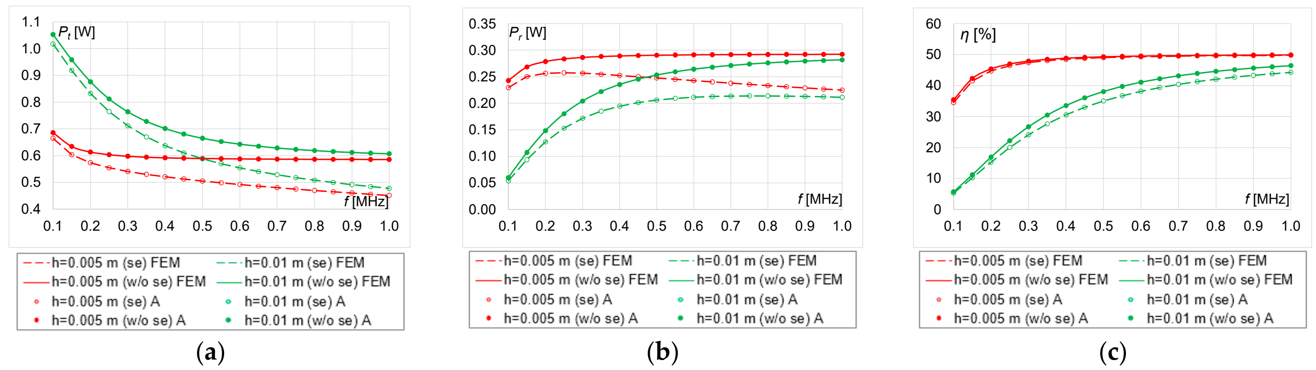

Figure 20. Results for n = 40 for the cases with and without skin effect: (**a**) P_t, (**b**) P_r, (**c**) η.

Regardless of n, the P_t power decreases over the entire frequency range (Figures 17a, 18a, 19a and 20a). As f and n increases, the influence of the skin effect on the transmitter power increases. The P_r power values stabilize after reaching the maximum value (Figures 17b, 18b, 19b and 20b). However, at h = 0.01 m, the P_r power increases over the entire frequency range. The skin effect reduces the P_r power as the frequency increases. The higher the frequency, the greater the influence of the skin effect on the P_r power values. Regardless of n and h, the P_r power is always higher for the case without skin effect. The differences in values for the cases with and without the skin effect are approximately 23%, regardless of n, at h = 0.005 m and at f = 1 MHz.

In this operation procedure, η tends to a maximum of 50% then maximum power is supplied to the load (Figures 17c, 18c, 19c and 20c). At h = 0.01 m, η increases over the entire analyzed frequency range, regardless of n. As n increases, the influence of the skin effect on the efficiency of the system decreases (Figures 19c and 20c). The greatest influence of the skin effect can be observed at h = 0.005 m and n = 10, 20 (Figures 17c and 18c).

3.3.2. Results for a Large Coil

The following characteristics are shown in Figures 21–23: P_t and P_r powers, and η at distances 0.0125 m and 0.025 m for cases with and without skin effect.

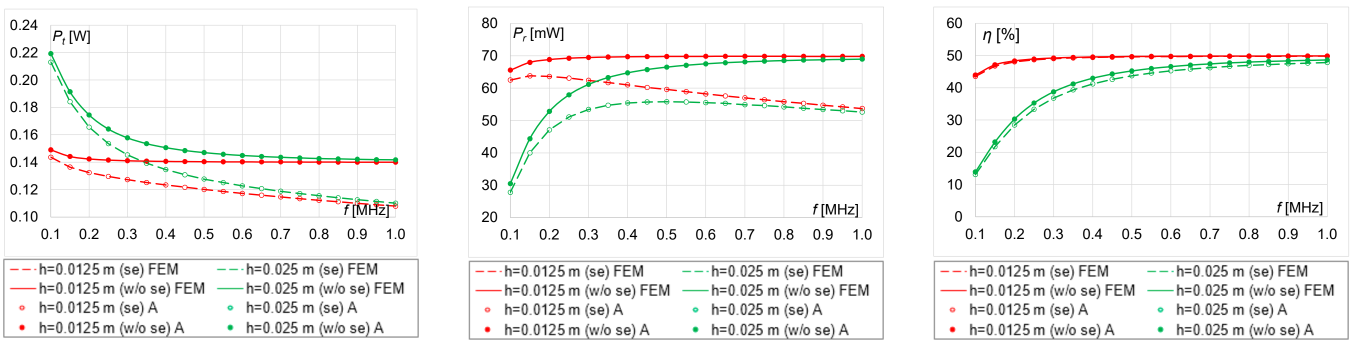

(**a**) (**b**) (**c**)

Figure 21. Results for n = 50 for the cases with and without skin effect: (**a**) P_t, (**b**) P_r, (**c**) η.

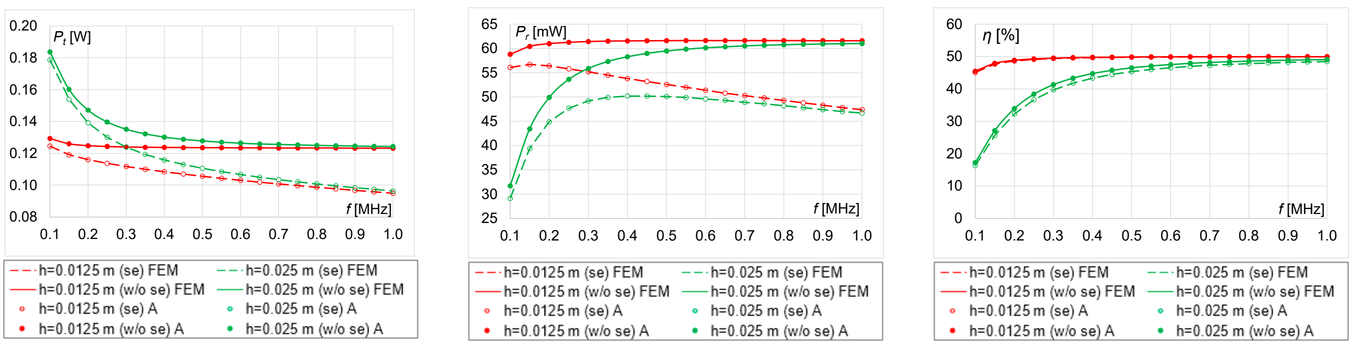

(**a**) (**b**) (**c**)

Figure 22. Results for n = 60 for the cases with and without skin effect: (**a**) P_t, (**b**) P_r, (**c**) η.

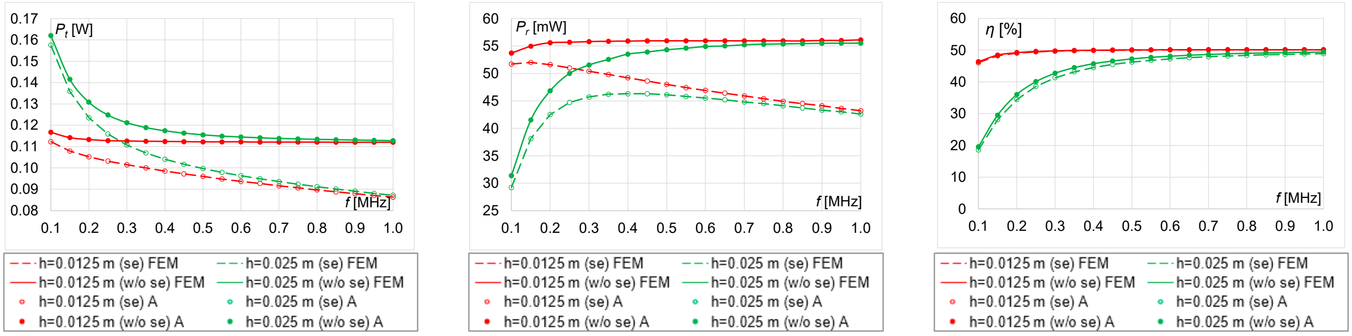

(**a**) (**b**) (**c**)

Figure 23. Results for n = 70 for the cases with and without skin effect: (**a**) P_t, (**b**) P_r, (**c**) η.

Regardless of n, the P_t power decreases over the entire frequency range (Figures 21a, 22a and 23a). As n increases, the transmitter power decreases. The influence of the skin effect on the P_t power is greater with increasing f and n, and at the frequency of 1 MHz, it is comparable, regardless of the distance between the coils.

The P_r power stabilizes after reaching the maximum value (Figures 21b, 22b and 23b). As n increases, the P_r power decreases. As the frequency increases, the skin effect reduces the receiver power. The higher the frequency, the greater the influence of the skin effect on the values of P_r power. Regardless of n and h, the P_r power is always higher for the case without skin effect.

In this operation procedure, η tends to a maximum of 50%, and then the maximum power is delivered to the load (Figures 21c, 22c and 23c). The influence of the skin effect on η of the WPT system at h = 0.0125 m is negligible. However, at h = 0.025 m, the influence of the skin effect on η is the greatest over the frequency range of 0.2 MHz to 0.5 MHz.

3.4. Distribution of Magnetic Flux Density

Example distribution of magnetic flux density (**B**) is presented in xz cut plane of the model along with normalized vectors, showing the direction of **B** (Figure 24). The Tx coil is located at z = 0 while Rx is at z = 0.005 m.

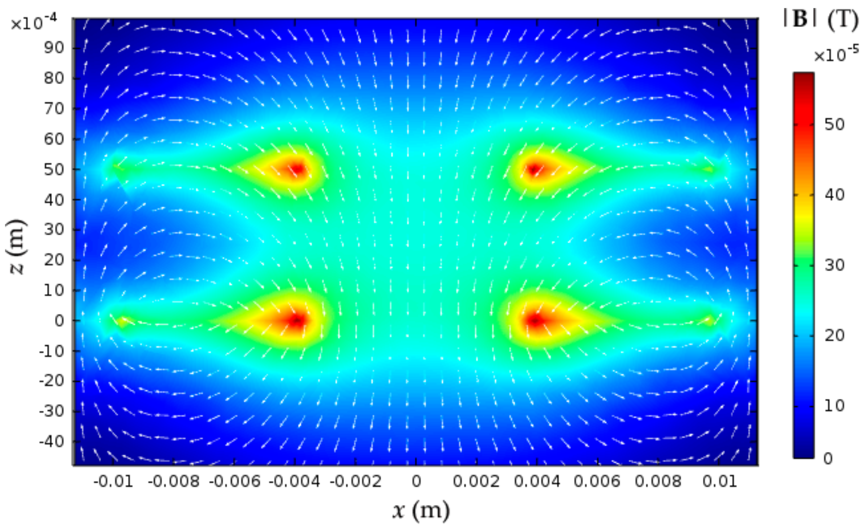

Figure 24. Magnetic flux density distribution (color) and its normalized vectors (white arrows) in xz surface, for the model with maximized efficiency at r = 0.01 m, h = 0.005 m, n = 30, and f = 1 MHz.

4. Conclusions

Alternating current generates lower losses, making it much better suited to transmit power over long distances. For the same reason, wireless technologies are unlikely to completely replace wired solutions. The idea of wireless energy transmission has been discussed for many years, but recently there have been more and more experiments confirming the practical possibility of using such a solution. If all efforts lead to progress, we expect WPT technology to spread on a larger scale and have a huge impact on everyday life.

In this article a WPT system was presented, in which the maximum efficiency and maximum load power operating procedures have been solved. In the article, the analytical and numerical approaches were shown. Both proposed methods of analysis were suitable for evaluating the properties of the WPT system and allowed for a quick estimation of power and efficiency. Since thin wires are used in planar coils, the influence of the skin effect on system efficiency is an important part of the analysis. The article presents an analysis of this problem on the example of many variants that differ in the geometry of the system. This analysis was focused on the maximum efficiency and power of the load.

With a detailed and multi-variant analysis, it can be concluded that the skin effect is acceptable. At 1 MHz, the efficiency losses for the small coil are max. up to 5%, and for the large coil, they are up to 9% (Table 7). The greatest decrease in efficiency occurs for a larger distance between the coils, i.e., $h = r$. With increasing distance, the efficiency decreases, and the skin effect further reduces the efficiency value. With a higher number of turns, the skin effect has less effect on the WPT system.

Analysis of the results of the maximum power of the receiver showed that the skin effect is comparable for both coils ($r = 0.01$ m, $r = 0.025$ m) at a smaller distance ($h = r/2$). However, with greater distance between the coils, the power values decrease as the number of turns increases.

The influence of the skin effect on the maximum efficiency and power of the receiver was analysed. Based on the results, the greatest influence of the skin effect occurred at 1 MHz:

(a) in the maximum efficiency procedure:
   (1) for the small coil ($r = 0.01$ m):
      - $n = 10$: 6% ($h = 0.005$ m), 8% ($h = 0.01$ m);
      - $n = 20$: 3% ($h = 0.005$ m), 9% ($h = 0.01$ m);
      - $n = 30$: 3% ($h = 0.005$ m), 7% ($h = 0.01$ m);
      - $n = 40$: 3% ($h = 0.005$ m), 7% ($h = 0.01$ m);
   (2) for the large coil ($r = 0.025$ m):
      - $n = 50$: 1% ($h = 0.0125$ m), 5% ($h = 0.025$ m);
      - $n = 60$: 1% ($h = 0.0125$ m), 5% ($h = 0.025$ m);
      - $n = 70$: 1% ($h = 0.0125$ m), 4% ($h = 0.025$ m);

(b) in the maximum load power procedure:
   (3) for the small coil ($r = 0.01$ m):
      - $n = 10$: 178 mW ($h = 0.005$ m), 195 mW ($h = 0.01$ m);
      - $n = 20$: 100 mW ($h = 0.005$ m), 107 mW ($h = 0.01$ m);
      - $n = 30$: 77 mW ($h = 0.005$ m), 80 mW ($h = 0.01$ m);
      - $n = 40$: 67 mW ($h = 0.005$ m), 71 mW ($h = 0.01$ m);
   (4) for the large coil ($r = 0.025$ m):
      - $n = 50$: 16 mW ($h = 0.0125$ m), 16 mW ($h = 0.025$ m);
      - $n = 60$: 15 mW ($h = 0.0125$ m), 14 mW ($h = 0.025$ m);
      - $n = 70$: 13 mW ($h = 0.0125$ m), 13 mW ($h = 0.025$ m).

It is well known that coil resistance increases with increasing frequency due to the skin effect. Choosing the wire diameter smaller than the skin depth could minimize the skin effect losses. However, this causes an increase in the resistance of the coil and heating of the wire from which the coil is wound. As a result, the efficiency and power of the receiver in the WPT system also decrease. The author plans to consider this case in detail in the next article to assess whether it is better to accept skin effect losses or reduce the wire diameter to eliminate them.

Funding: The printing of the article was financed from the **ZIREG project—Integrated Program of the Bialystok University of Technology for Regional Development**, contract no. POWR.03.05.00-00-ZR22/18. Project co-financed by the European Union from the European Social Fund under the Knowledge Education Development Operational Program 2014–2020.

Data Availability Statement: Not applicable.

Conflicts of Interest: The author declares no conflict of interest.

References

1. Sun, L.; Ma, D.; Tang, H. A review of recent trends in wireless power transfer technology and its applications in electric vehicle wireless charging. *Renew. Sustain. Energy Rev.* **2018**, *91*, 490–503. [CrossRef]
2. Alberto, J.; Reggiani, U.; Sandrolini, L.; Albuquerque, H. Fast calculation and analysis of the equivalent impedance of a wireless power transfer system using an array of magnetically coupled resonators. *PIER B* **2018**, *80*, 101–112. [CrossRef]
3. Batra, T.; Schaltz, E.; Ahn, S. Effect of ferrite addition above the base ferrite on the coupling factor of wireless power transfer for vehicle applications. *J. Appl. Phys.* **2015**, *117*, 17D517. [CrossRef]
4. Yang, Y.; El Baghdadi, M.; Lan, Y.; Benomar, Y.; Van Mierlo, J.; Hegazy, O. Design Methodology, Modeling, and Comparative Study of Wireless Power Transfer Systems for Electric Vehicles. *Energies* **2018**, *11*, 1716. [CrossRef]
5. Inoue, K.; Kusaka, K.; Itoh, J.I. Reduction in radiation noise level for inductive power transfer systems using spread spectrum techniques. *IEEE Trans. Power Electron.* **2018**, *33*, 3076–3085. [CrossRef]
6. Kan, T.; Mai, R.; Mercier, P.P.; Mi, C.C. Design and analysis of a three-phase wireless charging system for lightweight autonomous underwater vehicles. *IEEE Trans. Power Electron.* **2017**, *3*, 6622–6632. [CrossRef]
7. Tang, S.C.; Lun, T.L.T.; Guo, Z.; Kwok, K.W.; McDannold, N.J. Intermediate range wireless power transfer with segmented coil transmitters for implantable heart pumps. *IEEE Trans. Power Electron.* **2017**, *32*, 3844–3857. [CrossRef]
8. Li, X.; Zhang, H.; Peng, F.; Li, Y.; Yang, T.; Wang, B.; Fang, D. A wireless magnetic resonance energy transfer system for micro implantable medical sensors. *Sensors* **2012**, *12*, 10292–10308. [CrossRef]
9. Fitzpatrick, D.C. *Implantable Electronic Medical Devices*; Academic Press: San Diego, CA, USA, 2014; pp. 7–35.
10. Kang, S.H.; Choi, J.H.; Jung, C.W. Magnetic resonance wireless power transfer using three-coil system with single planar receiver for laptop applications. *IEEE Trans. Consum. Electron.* **2015**, *61*, 160–166.
11. Barman, S.D.; Reza, A.W.; Kumar, N.N.; Karim, M.E.; Munir, A.B. Wireless powering by magnetic resonant coupling: Recent trends in wireless power transfer system and its applications. *Renew. Sust. Energ. Rev.* **2015**, *51*, 1525–1552. [CrossRef]
12. Sugino, M.; Kondo, H.; Takeda, S. Linear motion type transfer robot using the wireless power transfer system. In Proceedings of the 2016 International Symposium on Antennas and Propagation (ISAP), Okinawa, Japan, 24–28 October 2016; pp. 508–509.
13. Wu, Q.; Tao, M.; Kwan Ng, D.W.; Chen, W.; Schober, R. Energy-efficient resource allocation for wireless powered communication networks. *IEEE Trans. Wirel. Commun.* **2016**, *15*, 2312–2327. [CrossRef]
14. Choroszucho, A.; Butryło, B. Local attenuation of electromagnetic field generated by wireless communication system inside the building. *Przegląd Elektrotechniczny* **2011**, *87*, 123–127.
15. Vamvakas, P.; Tsiropoulou, E.E.; Vomvas, M.; Papavassiliou, S. Adaptive power management in wireless powered communication networks: A user-centric approach. In Proceedings of the IEEE 38th Sarnoff Symposium, Newark, NJ, USA, 18–20 September 2017; pp. 1–6.
16. Khang, S.T.; Lee, D.J.; Hwang, I.J.; Yeo, T.D.; Yu, J.W. Microwave power transfer with optimal number of rectenna arrays for midrange applications. *IEEE Antennas Wirel. Propag. Lett.* **2018**, *17*, 155–159. [CrossRef]
17. De Santi, C.; Meneghini, M.; Caria, A.; Dogmus, E.; Zegaoui, M.; Medjdoub, F.; Kalinic, B.; Cesca, T.; Zanoni, E. GaN-based laser wireless power transfer system. *Materials* **2018**, *11*, 153. [CrossRef]
18. Li, Q.; Deng, Z.; Zhang, K.; Wang, B. Precise attitude control of multirotary-joint solar-power satellite. *J. Guid. Control Dyn.* **2018**, *41*, 1435–1442. [CrossRef]
19. Micus, S.; Padani, L.; Haupt, M.; Gresser, G.T. Textile-Based Coils for Inductive Wireless Power Transmission. *Appl. Sci.* **2021**, *11*, 4309. [CrossRef]
20. Luo, Z.; Wei, X. Analysis of square and circular planar spiral coils in wireless power transfer system for electric vehicles. *IEEE Trans. Ind. Electron.* **2018**, *65*, 331–341. [CrossRef]
21. Chen, L.; Liu, S.; Zhou, Y.C.; Cui, T.J. An optimizable circuit structure for high-efficiency wireless power transfer. *IEEE Trans. Ind. Electron.* **2013**, *60*, 339–349. [CrossRef]
22. Sołjan, Z.; Hołdyński, G.; Zajkowski, M. CPC-Based Minimizing of Balancing Compensators in Four-Wire Nonsinusoidal Asymmetrical Systems. *Energies* **2021**, *14*, 1815. [CrossRef]
23. Raven, M.S. Skin effect in the time and frequency domain—Comparison of power series and Bessel function solutions. *J. Phys. Commun.* **2018**, *3*, 035028. [CrossRef]
24. Abou Houran, M.; Yang, X.; Chen, W. Free Angular-Positioning Wireless Power Transfer Using a Spherical Joint. *Energies* **2018**, *11*, 3488. [CrossRef]
25. Lee, S.-H.; Lorenz, R.D. Development and validation of model for 95%-efficiency 220-w wireless power transfer over a 30-cm air gap. *IEEE Trans. Ind. Appl.* **2011**, *47*, 2495–2504. [CrossRef]

26. Raven, M.S. Experimental measurements of the skin effect and internal inductance at low frequencies. *Acta Tech.* **2016**, *60*, 51–69.
27. Steckiewicz, A. Efficient Transfer of the Medium Frequency Magnetic Field Using Anisotropic Metamaterials. *Energies* **2023**, *16*, 334. [CrossRef]
28. Xun, J.-H.; Mu, Y.; Zhang, K.; Liu, H.; Li, L. The Efficiency Improvement of Multiple Receivers in Wireless Power Transmission by Integrating Metasurfaces. *Materials* **2022**, *15*, 6943. [CrossRef]
29. Villa, J.L.; Sallan, J.; Sanz Osorio, J.F.; Llombart, A. High-misalignment tolerant compensation topology for icpt systems. *IEEE Trans. Ind. Electron.* **2012**, *59*, 945–951. [CrossRef]
30. Zhong, W.; Lee, C.K.; Hui, S.Y.R. General analysis on the use of Tesla's resonators in domino forms for wireless power transfer. *IEEE Trans. Ind. Electron.* **2013**, *60*, 261–270. [CrossRef]
31. Nguyen, B.X.; Vilathgamuwa, D.M.; Foo, G.; Ong, A.; Sampath, P.K.; Madawala, U.K. Cascaded multilevel converter based bidirectional inductive power transfer (BIPT) system. In Proceedings of the 2014 International Power Electronics Conference (IPEC-Hiroshima 2014—ECCE ASIA), Hiroshima, Japan, 18–21 May 2014; pp. 2722–2728.
32. Hao, H.; Covic, G.A.; Boys, J.T. A parallel topology for inductive power transfer power supplies. *IEEE Trans. Power Electron.* **2014**, *29*, 1140–1151. [CrossRef]
33. Mai, R.; Lu, L.; Li, Y.; Lin, T.; He, Z. Circulating Current Reduction Strategy for Parallel-Connected Inverters Based IPT Systems. *Energies* **2017**, *10*, 261. [CrossRef]
34. He, H.; Liu, Y.; Wei, B.; Wu, X.; Jiang, C.; Jiang, B.; Wei, C. Phase synchronization and current sharing strategy for multiple overlapped transmitters IPT system. *Energy Rep.* **2022**, *8*, 1103–1111. [CrossRef]
35. Awai, I.; Komori, T. A simple and versatile design method of resonator-coupled wireless power transfer system. In Proceedings of the 2010 International Conference on Communications, Circuits and Systems, ICCCAS 2010—Proceedings, Chengdu, China, 28–30 July 2010; pp. 616–620.
36. Lee, W.-S.; Son, W.-I.; Oh, K.-S.; Yu, J.-W. Contactless energy transfer systems using antiparallel resonant loops. *IEEE Trans. Ind. Electron.* **2013**, *60*, 6093746. [CrossRef]
37. Wang, B.; Yerazunis, W.; Teo, K.H. Wireless power transfer: Metamaterials and array of coupled resonators. *Proc. IEEE* **2013**, *101*, 1359–1368. [CrossRef]
38. Taflove, A.; Hagness, S.C. *Computational Electrodynamics: The Finite-Difference Time-Domain Method*; Artech House: Boston, MA, USA, 2005.
39. Choroszucho, A.; Butryło, B. Inhomogeneities and dumping of high frequency electromagnetic field in the space close to porous wall. *Przegląd Elektrotechniczny* **2012**, *88*, 263–266.
40. Zienkiewicz, O.C.; Taylor, R.L.; Zhu, J.Z. *The Finite Element Method: Its Basis & Fundamentals*, 7th ed.; Butterworth-Heinemann: Oxford, UK, 2013.
41. *Introduction to the RF Module, COMSOL*; Version: COMSOL 4.3b; COMSOL Inc.: Burlington, MA, USA, 2013.
42. *RF Module User's Guide, COMSOL*; Version: COMSOL 4.3b; COMSOL Inc.: Burlington, MA, USA, 2013.
43. Stankiewicz, J.M.; Choroszucho, A. Efficiency of the Wireless Power Transfer System with Planar Coils in the Periodic and Aperiodic Systems. *Energies* **2022**, *15*, 115. [CrossRef]
44. Mohan, S.S.; del Mar Hershenson, M.; Boyd, S.P.; Lee, T.H. Simple Accurate Expressions for Planar Spiral Inductances. *IEEE J. Solid-State Circuits* **1999**, *34*, 1419–1424. [CrossRef]
45. Liu, S.; Su, J.; Lai, J. Accurate Expressions of Mutual Inductance and Their Calculation of Archimedean Spiral Coils. *Energies* **2019**, *12*, 2017. [CrossRef]